Dynamic localization and transport in complex crystals

S. Longhi
Dipartimento di Fisica and Istituto di Fotonica e Nanotecnologie del CNR, Politecnico di Milano, Piazza L. da Vinci 32, I-20133 Milano, Italy

The behavior of a Bloch particle in a complex crystal with $\mathcal{PT}$ symmetry subjected to a sinusoidal ac force is theoretically investigated. For unbroken $\mathcal{PT}$ symmetry and in the single-band approximation, it is shown that time reversal symmetry of the ac force preserves the reality of the quasienergy spectrum. Like in ordinary crystals, exact band collapse, corresponding to dynamic localization, is attained for a sinusoidal band shape. The wave packet dynamics turns out to be deeply modified at the $\mathcal{PT}$ symmetry breaking point, where band merging occurs and Bragg scattering in the crystal becomes highly non-reciprocal.

PACS numbers: 73.23.Ad, 11.30.Er, 72.10.Bg

I. INTRODUCTION

The dynamics of matter or classical waves in periodic potentials subjected to external dc or ac forces is strongly influenced by Bragg scattering, which is responsible for such important effects as Bloch oscillations (BOs) and dynamic localization (DL). Dynamic localization was originally proposed by Dunlap and Kenkre [1] as a suppression of the broadening of a charged-particle wave packet as it moves along a tight-binding lattice driven by a sinusoidal ac electric field. DL was then explained in terms of quasienergy band collapse [2], and the general conditions of DL beyond the nearest-neighboring tight-binding (NNTB) approximation used by Dunlap and Kenkre were subsequently investigated in Ref.[3]. The interest on DL has been recently renewed since the first experimental observations of DL have been reported for matter waves trapped in dynamical optical lattices [4–6], and for light waves in curved waveguide arrays [7–11]. Matter or light waves may also interact with complex potentials. Complex crystals for matter waves emerge, for instance, in the near resonant interaction of light with open two-level systems [12], whereas in optics complex crystals are realized by waveguide arrays that include gain and/or loss regions [13]. As compared to ordinary crystals, complex crystals exhibit some unique properties, such as violation of the Friedel's law of Bragg scattering and nonreciprocal diffraction [12–14]. A special class of complex crystals is provided by complex potentials possessing parity-time ($\mathcal{PT}$) symmetry [13, 15, 16]. An important property of $\mathcal{PT}$ crystals is to admit of an entirely real-valued energy spectrum below a phase transition (symmetry-breaking) point, in spite of the non-Hermiticity of the underlying Hamiltonian [15]. A recent study on BOs in $\mathcal{PT}$ crystals [17] has shown that the common wisdom of coherent quantum transport in a crystal is greatly modified when dealing with a complex crystal.

It is the aim of this work to investigate the coherent motion of wave packets in a complex $\mathcal{PT}$ crystal driven by an ac-like force. In particular, it is shown that in the unbroken $\mathcal{PT}$ symmetry region time reversal symmetry of the ac-like force preserves the reality of the quasienergy spectrum, and that a full band collapse, corresponding to dynamic localization, occurs within the single-band and NNTB approximations like in ordinary crystals. However, the transport properties of the lattice are deeply modified at the $\mathcal{PT}$ symmetry breaking, where Bragg scattering in the crystal becomes highly non-reciprocal. In the following analysis, we will consider specifically wave packets in a photonic lattice system [7, 11, 13, 17], however the results can be applied to other lattice realizations, such as to matter wave tunneling in dynamic complex optical lattices.

II. DYNAMIC LOCALIZATION IN COMPLEX CRYSTALS WITH UNBROKEN $\mathcal{PT}$ SYMMETRY

In optics, the coherent motion of charged quantum particles in periodic potentials driven by an ac electric field can be mimicked by the propagation of light waves in a periodically-curved photonic lattice [7, 18]. In the scalar and paraxial approximations, light propagation at wavelength λ in the lattice is described by the Schrödinger-type wave equation

$$i\lambda\partial_z\psi = -\frac{\lambda^2}{2n_s}\partial_x^2\psi + V(x)\psi - Fx\psi \equiv (\mathcal{H}_0 - Fx)\psi. \quad (1)$$

where $\lambda = \lambda/(2\pi)$ is the reduced wavelength, n_s is the substrate refractive index, $V(x) = n_s - n(x)$ is the potential, $n(x) = n(x+a)$ is the refractive index profile of the lattice (spatial period a), and $F = F(z)$ is a fictitious refractive index gradient proportional to the local waveguide axis curvature which mimics the action of a driving force [18]. In particular, a sinusoidal ac-like force is simply mimicked by a sinusoidal bending profile of the waveguides [7]. In a complex lattice, the refractive index is complex, and the $\mathcal{PT}$ symmetry requirement $V(-x) = V^*(x)$ corresponds to suitable combinations of optical gain and loss regions in the lattice as discussed in [13]. The real and imaginary parts of the potential are denoted by $V_R(x)$ and $\alpha V_I(x)$, respectively, where $\alpha \geq 0$ is a dimensionless parameter that measures

the anti-Hermitian strength of $\mathcal{H}_0$. The spectrum of $\mathcal{H}_0$ turns out to be real-valued for $\alpha < \alpha_c$, where $\alpha_c \geq 0$ corresponds to the transition from unbroken to broken $\mathcal{PT}$ symmetry. Numerical studies generally show that for $\alpha < \alpha_c$ the spectrum is composed by bands separated by gaps like in an ordinary crystal, whereas for $\alpha \geq \alpha_c$ band merging is observed with the appearance of pairs of complex-conjugate eigenvalues [13, 16]. For instance, for the potential defined by

$$V_R(x) = V_0 \cos(2\pi x/a) \ , \ \ V_I(x) = V_0 \sin(2\pi x/a), \quad (2)$$

one has $\alpha_c = 1$ [13].

In this section we consider the unbroken symmetry phase, i.e. the case $\alpha < \alpha_c$. As recently shown in Ref.[17], for $\alpha < \alpha_c$ the motion of a Bloch particle in presence of an external dc force F can be described following the same lines as in ordinary crystals by expanding the field $\psi(x,z)$ as a superposition of Bloch-Floquet eigenfunctions $\phi_n(x,\kappa) = u_n(x,\kappa)\exp(i\kappa x)$ of $\mathcal{H}_0$, where the wave number κ varies in the first Brillouin zone, i.e. $-k_B/2 \leq \kappa < k_B/2$, $k_B = 2\pi/a$ is the Bragg wave number, n is the band index, and $u_n(x,\kappa)$ is the periodic part of the Bloch-Floquet eigenfunction. After setting $\psi(x,z) = \sum_n \int d\kappa c_n(\kappa,z)\phi_n(\kappa,z)$ and assuming normalized eigenfunctions such that $\int dx \phi^*_{n'}(-x,-\kappa')\phi_n(x,\kappa) = \mathcal{D}_n \delta_{n,n'}\delta(\kappa-\kappa')$ with $\mathcal{D}_n = \pm 1$, the evolution equations for the spectral coefficients $c_n(\kappa,z)$ read [17]

$$i\lambda\left(\partial_z + \frac{F}{\lambda}\partial_\kappa\right) c_n = E_n(\kappa)c_n - F\mathcal{D}_n \sum_l X_{n,l}(\kappa)c_l \quad (3)$$

where $E_n(\kappa)$ is the energy of $\phi_n(x,\kappa)$ [with $E_n(-\kappa) = E_n(\kappa)$] and $X_{n,l}(\kappa) \equiv (2\pi i/a)\int_0^a dx u^*_n(-x,-\kappa)\partial_\kappa u_l(x,\kappa)$. The off-diagonal elements $X_{n,l}$ $(n \neq l)$ in Eq.(3) are responsible for interband transitions, i.e. Zener tunneling (ZT). If bands n and l are separated by a large gap and the ac force $F(z)$ is small enough such that $|FX_{n,l}(\kappa)| \ll |E_n(\kappa) - E_l(\kappa)|$ in the entire Brillouin zone, ZT is negligible as in ordinary lattices and one can make the single-band approximation by setting $X_{n,l} \simeq 0$ for $n \neq l$ in Eq.(3). In the single-band approximation one thus obtains

$$i\lambda\left(\partial_z + \frac{F}{\lambda}\partial_\kappa\right) c(z,\kappa) = \left[E(\kappa) - iF(z)\Phi(\kappa)\right] c(\kappa,z) \quad (4)$$

where we omitted, for the sake of simplicity, the band index n and set $i\Phi(\kappa) \equiv \mathcal{D}_n X_{n,n}(\kappa)$. Because of the symmetry of $V(x)$, $\mathrm{Re}(u_n(k,x))$ and $\mathrm{Im}(u_n(k,x))$ have well defined and opposite parity under the inversion $x \to -x$; this implies that $\Phi(\kappa)$ is a real-valued function of κ, vanishing for a real potential (i.e. for $\alpha = 0$). As previously shown in [17], when a dc force F is applied to the crystal, from Eq.(4) it follows that the energy spectrum is described by a complex-valued Wannier-Stark ladder. The non-reality of the energy spectrum comes from the extra-term $\Phi(\kappa)$ in Eq.(4) and is physically due to the fact that the external dc force F breaks the $\mathcal{PT}$ symmetry of the full Hamiltonian $\mathcal{H} = \mathcal{H}_0 - Fx$. For an ac-like force with period $\Lambda = 2\pi/\omega$, because of the z-periodicity of the Hamiltonian its energy spectrum is replaced by a quasi-energy spectrum. Moreover, in the single-band approximation DL corresponds to a complete collapse of the quasi-energy band like in an ordinary crystal [2]. According to Floquet's theorem of periodic systems, the quasi-energy $\mathcal{E}(\kappa)$ for the n-th lattice band can be readily calculated by looking for a solution to Eq.(4) of the form $c(z,\kappa) = a(z,\kappa)\exp[-i\mathcal{E}(\kappa)z/\lambda]$ with $a(z+\Lambda,\kappa) = a(z,\kappa)$. One obtains

$$\mathcal{E}(\kappa) = \frac{1}{\Lambda}\int_0^\Lambda dz \left[E(\kappa') - iF(z)\Phi(\kappa')\right] \quad (5)$$

where we have set $\kappa' \equiv \kappa - k(\Lambda) + k(z)$ and $k(z) = (1/\lambda)\int_0^z d\xi F(\xi)$. Let us assume that the ac forcing $F(z)$ is an odd function with respect to some point z_0, i.e. that $F(z-z_0) = -F(z_0-z)$ for some z_0 in the oscillation cycle. This condition is satisfied, for instance, for the important case of an harmonic (e.g. sinusoidal or cosinusoidal) ac driving force, originally considered by Dunlap and Kenkre [1] and that will be assumed in the following. Owing to this additional temporal symmetry on the driving force, which is absent for the BO problem [17], a real-valued quasi-energy spectrum for the non-Hermitian time-periodic Hamiltonian $\mathcal{H}_0 - F(z)x$ is obtained. In fact, in this case the imaginary term on the right hand side of Eq.(5) vanishes after integration because $F(z)$ and $\Phi(\kappa')$ have opposite parity for the inversion $(z-z_0) \to -(z-z_0)$. The quasi-energy spectrum is thus real-valued and its expression takes the usual form as in a conventional crystal. DL corresponds to a collapse of the quasienergy band $\mathcal{E}(\kappa)$, i.e. to $d\mathcal{E}(\kappa)/d\kappa = 0$. For most driving fields like a sinusoidal field, DL can be attained exactly solely in the NNTB approximation, i.e. when the band shape $E(\kappa)$ is sinusoidal [3], $E(\kappa) = E_0 - \Delta\cos(\kappa a)$. In this case, assuming for the sake of definiteness a sinusoidal ac-like force $F(z) = F_0\cos(\omega z)$, the explicit form of the quasi-energy reads [2]

$$\mathcal{E}(\kappa) = E_0 - \Delta J_0\left(\frac{F_0 a}{\lambda\omega}\right)\cos(\kappa a). \quad (6)$$

Band collapse, leading to DL, is thus attained when $J_0(F_0 a/\lambda\omega) = 0$ [1, 2, 7].

To check the correctness of the analysis, we investigated DL for the complex crystal $V(x) = V_0[\cos(2\pi x/a) + i\alpha\sin(2\pi x/a)]$ in the unbroken $\mathcal{PT}$ symmetry phase ($\alpha < 1$) by a direct numerical analysis of Eq.(1) using a pseudo-spectral split-step method with absorbing boundary conditions. Figure 1 shows a typical example of band diagram below the phase transition point ($\alpha = 0.3$), numerically computed by a spectral analysis of the Hamiltonian $\mathcal{H}_0$. Note that the lowest band of the array is with excellent accuracy approximated by a sinusoidal curve and turns out to be separated by a large gap from the second

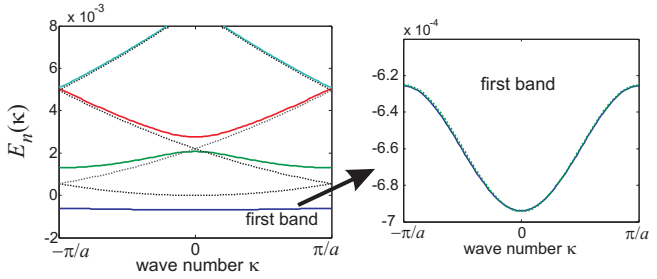

FIG. 1: (color online) Band diagram of the complex potential defined by Eq.(2) for parameter values $\lambda = 633$ nm, $a = 8$ μm, $n_s = 1.42$, $V_0 = 0.002$, and $\alpha = 0.3$. The dotted curve shows, for comparison, the parabolic dispersion relation $E(\kappa) = (\lambda\kappa)^2/(2n_s)$, folded inside the first Brillouin zone, corresponding to the critical case $\alpha = \alpha_c = 1$. The picture on the right hand side is an enlargement of the lowest band (solid curve), fitted by a sinusoidal curve (dotted curve), almost overlapped with the solid one.

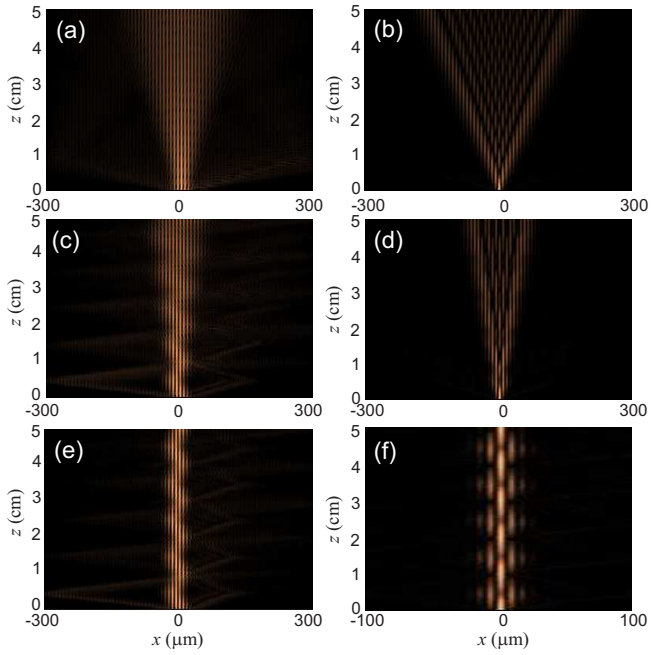

FIG. 2: (color online) Wave packet broadening (discrete diffraction) and dynamic localization in the lattice of Fig.1 for broad beam excitation at normal incidence (left panels) and for single site excitation at normal incidence (right panels). In (a) and (b), the external force is absent ($F_0 = 0$). In (c), (d) a sinusoidal force with period $\Lambda = 1$ cm and amplitude $F_0 = 13.32$ μm^{-1}, corresponding to $\Gamma = 1.684$, is applied. In (e) and (f), the forcing amplitude is increased to $F_0 = 19.03$ μm^{-1}, corresponding to the DL condition $\Gamma = 2.405$.

band. DL is thus expected to occur provided that the lattice is excited in its lowest order band. Figures 2(a) and (b) show a typical spreading (discrete diffraction) of a Gaussian wave packet $\psi(x,0) = \exp(-x^2/w^2)$ in the absence of the external force, for either a broad Gaussian beam that excites at normal incidence a few lattice sites at $z = 0$ [$2w = 5a$, Fig.2(a)], and a narrow Gaussian beam that excites at normal incidence a single well of the lattice [$2w = 2a/3$, Fig.2(b)]. In both cases, the lowest band of the array is mainly excited, as discussed e.g. in [8]. After application of the sinusoidal force [Figs.2(c-f)], suppression of beam diffraction and self-imaging effects are clearly observed when period and amplitude of forcing satisfy the condition $\Gamma \equiv F_0 a/(\lambda\omega) = 2.405$ (first zero of Bessel J_0 function), as shown in Figs.2(e) and (f).

III. WAVE PACKET DYNAMICS AT THE $\mathcal{PT}$ SYMMETRY-BREAKING POINT

As α is increased to reach and cross the $\mathcal{PT}$ symmetry-breaking point α_c, gap narrowing till band merging, associated to the appearance of pairs of complex-conjugate eigenvalues, is observed [13]. For instance, for the potential defined by Eq.(2), at the transition point the band diagram is given by the free-particle energy dispersion curve $E = \lambda^2\kappa^2/(2n_s)$, periodically folded inside the first Brillouin zone [13] (see the dotted curve in Fig.1). In this case, as previously noticed for BOs [17], wave packet transport is deeply modified and can not be described by means of the canonical model (3) introduced in the previous section. From a physical viewpoint, this is related to the highly non-reciprocal behavior of Bragg scattering in the crystal and violation of Friedel's law of Bragg diffraction for crystal inversion [12, 14]. As in Ref. [17], we limit here to consider the dynamical behavior of a broad wave packet in the complex lattice defined by Eq.(2) at $\alpha = \alpha_c = 1$, i.e. $V(x) = V_0 \exp(ik_B x)$, which enables a rather simple analytical and physical analysis. As opposed to Ref. [17], we assume here an ac-like force, namely $F(z) = F_0 \cos(\omega z)$. Figure 3 shows a few typical examples of wave packet dynamics as obtained by a numerical analysis of Eq.(1) when the lattice is excited at $z = 0$ with a broad Gaussian beam $\psi(x,0) = \exp(-x^2/w^2)$ for a fixed value of the ac modulation period $\Lambda = 2\pi/\omega$ and for increasing values of the amplitude F_0. For a small amplitude F_0, it turns out that the wave packet propagates as if the lattice were absent [Fig.3(a)], following an oscillatory path as predicted by the semiclassical analysis of Eq.(1) with $V = 0$. Owing to the external force, the mean wave packet momentum varies periodically according to $\lambda k(z) = \int_0^z d\xi F(\xi) = (F_0/\omega)\sin(\omega z)$. As the forcing F_0 reaches and crosses the critical value $F_c = k_B\lambda\omega/2$, new wave packets, arising from first-order Bragg diffraction, periodically bifurcate from the primary beam at propagation distances z satisfying the Bragg condition $k(z) = -k_B/2$ [see Figs.3(b) and 3(c)]. The mean momentum of the first-order diffracted wave packets differs from that of the primary wave packet by an additional term k_B, which explains the refraction of the first-order diffracted beams at the angle $\theta = dx/dz = k_B\lambda/n_s$ observed in Figs.3(b) and 3(c). At stronger forcing, namely for $F \geq 3F_c$, additional wave packets bifurcate from the

first-order wave packets at propagation distances z such that $k(z) = -3k_B/2$, as shown in Fig.3(d). These wave packets originate from second-order Bragg diffraction in the crystal and greatly complicate the pattern scenario. The mean momentum of second-order diffracted wave packets differs from that of the primary wave packet by the additional term $2k_B$, which explains the larger (twice) refraction angle of second-order diffracted beams as compared to that of first-order diffracted beams [see Fig.3(d)]. At even higher forcing, i.e. at $F \geq 5F_c$, new wave packets bifurcate from the second-order wave packets because of third-order Bragg diffraction at propagation distances z such that $k(z) = -5k_B/2$, and so on. The appearance of wave packets generated by Bragg diffraction at various orders is rather abrupt, as indicated by the behavior of the normalized beam power $P(z) = \int dx|\psi(x,z)|^2 / \int dx|\psi(x,0)|^2$ versus propagation distance z shown in the right panels of Fig.3.

The dynamical scenario observed in numerical simulations can be analytically captured by considering the limiting case of a plane wave exciting the crystal at $z = 0$ with initial wave number $k = 0$. In fact, the solution to Eq.(1) with the initial condition $\psi(x,0) = 1$ is given by the superposition of diffracted plane waves at different Bragg orders according to

$$\psi(x,z) = \sum_{n=0}^{\infty} a_n(z) \exp[ik(z)x + ink_B x - i\gamma_n(z)]. \quad (7)$$

In Eq.(7) we have set

$$k(z) = \frac{1}{\lambda} \int_0^z d\xi F(\xi) = \frac{F_0}{\lambda\omega} \sin(\omega z) \quad (8)$$

$$\gamma_n(z) = \frac{\lambda}{2n_s} \int_0^z d\xi \left[nk_0 + k(\xi)\right]^2, \quad (9)$$

whereas the amplitudes $a_n(z)$ are calculated from the recurrence relations

$$a_n(z) = -i\frac{V_0}{\lambda} \int_0^z d\xi a_{n-1}(\xi) \exp\left[i\gamma_n(z) - i\gamma_{n-1}(z)\right] \quad (10)$$

with $a_0(z) = 1$. The amplitude a_0 corresponds, in Fig.3, to the primary wave packet, and the independence of a_0 from z indicates that this wave packet propagates as if the lattice were absent. The amplitude a_1 corresponds to the first-order diffracted wave packets, a_2 to second-order diffracted wave packets, and so on. According to Eq.(10), a wave packet corresponding to Bragg diffraction at order n bifurcates from a wave packet of order $(n-1)$, and Bragg diffraction is effective provided that the phase difference $\varphi_n(z) = \gamma_n(z) - \gamma_{n-1}(z)$ entering in the exponential of the integral on the right-hand-side of Eq.(10) has a stationary point. The condition $d\varphi_n(z)/dz = 0$ is satisfied at propagation distances z_0 such that

$$k(z_0) = -k_B \left(n - \frac{1}{2}\right) \quad (n = 1, 2, 3, ...). \quad (11)$$

i.e. for a wave number that reaches the edge of the Bril-

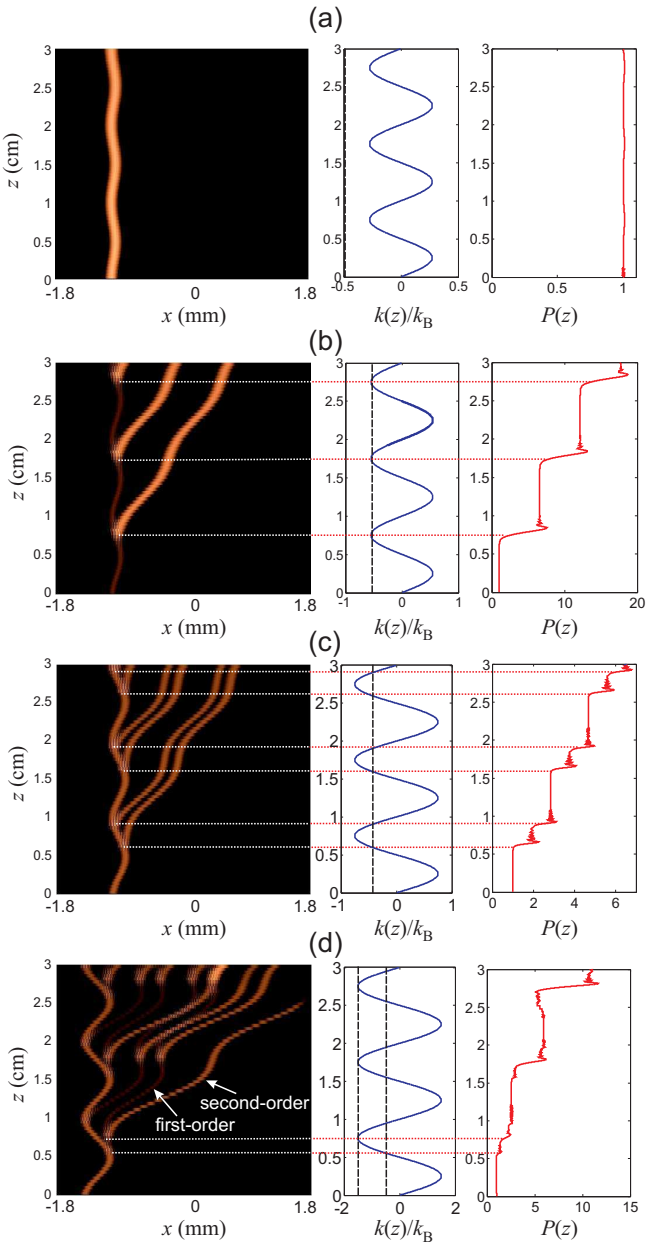

FIG. 3: (color online) Propagation of a broad Gaussian wave packet (input beam size $w = 80$ μm) in the complex lattice $V(x) = V_0 \exp(2\pi ix/a)$ for $V_0 = 0.0002$, $a = 6$ μm, $\lambda = 633$ nm, $n_s = 1.42$, subjected to a sinusoidal ac-like force $F(z) = F_0 \cos(2\pi z/\Lambda)$ with period $\Lambda = 1$ cm and with increasing values of force amplitude F_0: (a) $F_0/F_c = 0.5$, (b) $F_0/F_c = 1$, (c) $F_0/F_c = 1.5$, and (d) $F_0/F_c = 3$, where the critical forcing F_c is defined by Eq.(15). Left panels show snapshots of $|\psi(x,z)|$; the central panels depict the behavior of $k(z)$, normalized to the Bragg wave number k_B, as given by Eq.(8); the right panels show the evolution of normalized beam power $P(z)$. The horizontal dotted lines indicate the crossing points $z = z_0$ where new wave packets are generated by Bragg scattering. For the sake of clarity, in (d) only the first two crossing points are indicated. At the crossing points a rather abrupt increase of beam power $P(z)$ is observed. The crossing is linear in (b) and (d), and parabolic in (c).

louin zone. Note, however, that in Eqs.(7) and (11) n is a positive (but not a negative) integer number: this circumstance is a clear signature that Bragg scattering is highly non-reciprocal, a feature which is peculiar to the complex nature of the crystal [12, 14]. If the crossings of the stationary points are fast enough, $a_n(z)$ is basically constant far from the stationary points, with abrupt changes at $z = z_0$, namely

$$a_n(z_0^+) \simeq a_n(z_0^-) + R a_{n-1}(z_0) \tag{12}$$

where

$$R = -i\frac{V_0}{\lambda\!\!\!^{-}} \int d\xi \exp[i\varphi_n(\xi)] \tag{13}$$

and the integral on the right hand side of Eq.(13) is extended to the neighborhood of z_0. From these results one can readily explain the abrupt changes of the total beam power $P(z)$ observed in Fig.3 (right panels) at the crossing points shown in the central panels of Fig.3, the existence of a critical forcing F_c below which no bifurcating wave packets appear, as well as the occurrence of higher-order bifurcating wave packets and a dynamical scenario with increasing complexity as the amplitude of forcing is increased. In fact, according to Eqs. (8) and (11) the stationary points which generate the bifurcating wave packets of order n are obtained from the equation

$$\frac{F_0}{\lambda\!\!\!^{-}\omega} \sin(\omega z_0) = -\frac{k_B}{2}(2n-1), \tag{14}$$

which can be satisfied provided that the amplitude F_0 of forcing is larger than $F_c(2n-1)$, where

$$F_c = \frac{1}{2}\lambda\!\!\!^{-}\omega k_B \tag{15}$$

is the critical forcing amplitude. Therefore, for $F_0 < F_c$ no diffracted wave packets of any order are generated [Fig.3(a)], for $F_c \le F_0 < 3F_c$ first-order diffracted wave packets are generated, for $3F_c \le F_0 < 5F_c$ first-order and second-order wave packets are generated, and so on. The graphical determination of the stationary points is depicted in the central panels of Fig.3 as the crossing of the sinusoidal curve $k(z)/k_B$ with the vertical dashed lines $k/k_B = -0.5$ (for first-order Bragg diffraction) and $k/k_B = -1.5$ [for second-order Bragg diffraction, shown solely in Fig.3(d)]. Let ut discuss in some detail the generation of first-order diffracted wave packets ($n = 1$). For $F_c < F_0 < 3F_c$ [Fig.3(c)], in each ac oscillation cycle there are two stationary points, and the crossing is linear. Near each of the stationary points, $\varphi_1(z)$ can be thus approximated as $\varphi_1(z) = \varphi_1(z_0) + (1/2)(d^2\varphi_1/dz^2)(z-z_0)^2$, where the derivative $(d^2\varphi_1/dz^2)$ is calculated at the stationary point $z = z_0$. From Eq.(13), it follows that the amplitude factor $|R|$ of the generated diffracted beam after each stationary phase point can be approximately computed as

$$\begin{aligned} |R| &\simeq \frac{V_0}{\lambda\!\!\!^{-}} \left| \int_{-\infty}^{\infty} d\xi \exp\left(\frac{i}{2}\frac{d^2\varphi_1}{dz^2}\xi^2\right)\right| \\ &= \frac{V_0}{\lambda\!\!\!^{-}} \sqrt{\frac{2\pi n_s}{k_B\sqrt{F_0^2 - F_c^2}}}. \end{aligned} \tag{16}$$

In deriving Eq.(16), we have taken into account that $(d^2\varphi_1/dz^2) = F(z_0)k_B/n_s$, $|F(z_0)| = (F_0^2 - F_c^2)^{1/2}$ and $\int_{-\infty}^{\infty} d\xi \exp(i\xi^2) = \sqrt{i\pi}$. For parameter values used in the simulations of Fig.3(c), from Eq.(16) one has $|R| \simeq 0.95$, which is in excellent agreement with the staircase behavior of beam power $P(z)$ shown in the right panel of Fig.3(c). Equation (16) fails to predict the correct amplitude factor R when $F_0 \to F_c^+$, i.e. when the two crossing points in each ac oscillation cycle coalesce. For $F_0 = F_c$, the crossing is parabolic [see Fig.3(b), central panel], and $\varphi_1(z)$ in Eq.(13) should now be approximated as $\varphi_1(z) = \varphi_1(z_0) + (1/6)(d^3\varphi_1/dz^3)(z-z_0)^3$, where the derivative $(d^3\varphi_1/dz^3)$ is calculated at the crossing point $z = z_0$. In this case, in place of Eq.(16) one has

$$\begin{aligned} |R| &\simeq \frac{V_0}{\lambda\!\!\!^{-}} \left| \int_{-\infty}^{\infty} d\xi \exp\left(\frac{i}{6}\frac{d^3\varphi_1}{dz^3}\xi^3\right)\right| \\ &= \frac{V_0}{\lambda\!\!\!^{-}} 2\pi \mathrm{Ai}(0) \left(\frac{4n_s}{\lambda\!\!\!^{-}\omega^2 k_B^2}\right)^{1/3} \end{aligned} \tag{17}$$

where $\mathrm{Ai}(\xi)$ is the Airy function. In deriving Eq.(17), we have taken into account that $(d^3\varphi_1/dz^3) = (k_B/n_s)(dF/dz) = \lambda\!\!\!^{-}k_B^2\omega^2/(2n_s)$ at $z = z_0$, and $\int_{-\infty}^{\infty} d\xi \exp(i\xi^3/3) = 2\pi\mathrm{Ai}(0)$. For parameter values used in the simulations of Fig.3(b), from Eq.(17) one has $|R| \simeq 2.245$. Note that, with this amplitude factor, the staircase behavior of beam power $P(z)$ shown in the right panel of Fig.3(b) is reproduced with excellent accuracy.

IV. CONCLUSIONS

The coherent motion of a Bloch wave packet in a tight-binding lattice driven by an ac electric field is known to show a self-imaging effect that arises from quasi-energy band collapse of the time-periodic Hamiltonian. This phenomenon, referred to as dynamic localization [1, 2], has been recently observed for both matter and optical waves as a suppression of wave packet broadening in the lattice. In this work, we investigated theoretically the behavior of a Bloch particle in a complex crystal with $\mathcal{PT}$ symmetry subjected to a sinusoidal ac-like force. As compared to ordinary crystals, complex crystals exhibit some unique properties, such as violation of the Friedel's law of Bragg scattering and nonreciprocal diffraction. For an unbroken $\mathcal{PT}$ symmetry and in the single-band approximation, it has been shown that the quasi-energy spectrum of the time-periodic non-Hermitian Hamiltonian remains real-valued. In this regime, like in an ordinary crystal exact band collapse is possible within the

NNTB approximation, i.e. for a sinusoidal band shape. At the $\mathcal{PT}$ symmetry breaking transition point, band merging greatly modifies the wave packet dynamics as compared to an ordinary crystal. Here we have investigated in details the dynamics of a broad wave packet in the $\mathcal{PT}$-symmetric potential $V(x) = V_0 \exp(2\pi i x/a)$ and shown that the complexity of the dynamical scenario greatly increases as the strength of forcing is increased, with the appearance of a cascading of bifurcating wave packets. The main features observed in numerical simulations have been analytically explained by considering the Bragg scattering of a plane wave in the complex lattice subjected to the sinusoidal ac driving force. These results are complementary to the recent study of Bloch oscillations in complex crystals [17], and are expected to motivate further investigations aimed to explore the exotic transport properties o complex crystals.

[1] D.H. Dunlap and V. M. Kenkre, Phys. Rev. B **34**, 3625 (1986).
[2] M. Holthaus, Phys. Rev. Lett. **69**, 351 (1992).
[3] M.M. Dignam and C.M. de Sterke, Phys. Rev. Lett. **88**, 046806 (2002).
[4] K.W. Madison, M.C. Fischer, R.B. Diener, Q. Niu, and M.G. Raizen, Phys. Rev. Lett. **81**, 5093 (1998).
[5] H. Lignier, C. Sias, D. Ciampini, Y. Singh, A. Zenesini, O. Morsch, and E. Arimondo, Phys. Rev. Lett. **99**, 220403 (2007).
[6] A. Eckardt, M. Holthaus, H. Lignier, A. Zenesini, D. Ciampini, O. Morsch, and E. Arimondo, Phys. Rev. A **79**, 013611 (2009).
[7] S. Longhi, M. Marangoni, M. Lobino, R. Ramponi, P. Laporta, E. Cianci, and V. Foglietti, Phys. Rev. Lett. **96**, 243901 (2006).
[8] S. Longhi, M. Lobino, M. Marangoni, R. Ramponi, P. Laporta, E. Cianci, and V. Foglietti, Phys. Rev. B **74**, 155116 (2006).
[9] R. Iyer, J.S. Aitchison, J. Wan, M.M. Dignam, and C.M. de Sterke, Opt. Express **15**, 3212 (2007).
[10] F. Dreisow, M. Heinrich, A. Szameit, S. Doering, S. Nolte, A. Tünnermann, S. Fahr, and F. Lederer, Opt. Express **16**, 3474 (2008).
[11] A. Szameit, I.L. Garanovich, M. Heinrich, A.A. Sukhorukov, F. Dreisow, T. Pertsch1, S. Nolte, A. Tünnermann, and Yu. S. Kivshar, Nature Phys. **5**, 271 (2009).
[12] C. Keller, M.K. Oberthaler, R. Abfalterer, S. Bernet, J. Schmiedmayer, and A. Zeilinger, Phys. Rev. Lett. **79**, 3327 (1997).
[13] K.G. Makris, R. El-Ganainy, D.N. Christodoulides, and Z.H. Musslimani, Phys. Rev. Lett. **100**, 103904 (2008).
[14] M.V. Berry, J. Phys. A **31**, 3493 (1998); M.V. Berry and D.H.J. O'Dell, J. Phys. A **31**, 2093 (1998).
[15] C.M. Bender and S. Boettcher, Phys. Rev. Lett. **80**, 5243 (1998); A. Mostafazadeh, J. Math. Phys. **43**, 2814 (2002); C.M. Bender, Rep. Prog. Phys. **70**, 947 (2007).
[16] C.M. Bender, G.V. Dunne, P.N. Meisinger, Phys. Lett. A **252**, 272 (1999); H.F. Jones, Phys. Lett. A **262**, 242 (1999)
[17] S. Longhi, Phys. Rev. Lett. **103**, 123601 (2009).
[18] S. Longhi, Laser & Photon. Rev. **3**, 243 (2009).